Journal of Structural Geology, Vol. 9, No. 8, pp. 955 to 967, 1987
Printed in Great Britain

0191-8141/87 $03.00 + 0.00

Mechanisms of thrust faulting in the Gran Sasso chain, Central Apennines, Italy

FRANCESCA GHISETTI

Istituto di Scienze della Terra, Corso Italia 55, 95129 Catania, Italy

(*Received* 20 *May* 1986; *accepted in revised form* 10 *May* 1987)

Abstract—The Gran Sasso chain in Central Italy is made up of an imbricate stack of eight thrust sheets, which were emplaced over the Upper Miocene–Lower Pliocene Laga Flysch. The thrust sheets are numbered from 1 to 8 in order of their decreasing elevation in the tectonic stack, and their basal thrusts are numbered from T_1 to T_8, accordingly. On the basis of their different deformation features, the major thrust faults fall into three groups: (1) thrust faults marked by thick belts of incoherent gouges and breccia zones (T_1, T_2, T_3); (2) thrust faults characterized by a sharp plane which truncates folds that had developed in the footwall rocks (T_5, T_6); and (3) thrust faults truncating folds developed in both the hangingwall and footwall units, and bordered by foliated fault rocks (T_7). The deformation features observed for the different faults seem to vary because of two combined factors: (1) lithologic changes in the footwall and hangingwall units separated by the thrust faults; and (2) increasing amounts of deformation in the deepest portions of the imbricate stack. The upper thrust sheets (from 1 to 6) are characterized by massive calcareous and dolomitic rocks, they maintain a homoclinal setting and are truncated up-section by the cataclastic thrust faults. The lowermost thrust sheets (7 and 8) are characterized by a multilayer with competence contrasts, which undergoes shear-induced folding prior to the final emplacement of the thrust sheets. Bedding and axial planes of folds rotate progressively towards the T_5, T_6, T_7 and T_8 thrust boundaries, and are subsequently truncated by propagation of the brittle thrust faults. The maximum deformation is observed along the T_7 thrust fault, consistent with horizontal displacement that increases progressively from the uppermost to the lowermost thrust sheet in the tectonic stack. The axial planes of the folds developed in the hangingwall and footwall units are parallel to the T_7 thrust fault, and foliated fault rocks have developed. Field data and petrographic analysis indicate that cleavage fabrics in the fault rocks form by a combination of cataclasis, cataclastic flow and pressure-solution slip, associated with pervasive shearing along subtly distributed slip zones parallel to the T_7 thrust fault. The development of such fabrics at upper crustal levels creates easy-slip conditions in progressively thinner domains, which are regions of localized flow during the thrust sheet emplacement.

INTRODUCTION

THE GRAN SASSO chain in Central Italy is defined by an E–W system of imbricate carbonate thrust sheets which were emplaced over the Upper Miocene–Lower Pliocene sequences of the Laga Flysch (Fig. 1). At present, the chain is bounded by the 'Ancona-Anzio' and Sibillini thrust system to the west and is linked to the Morrone thrust front to the east. The E–W orientation and the northern vergence of the Gran Sasso chain are unique features in the Central Apennines, where tectonic transport towards the Adriatic foredeep has been generally accomplished by eastward verging, NW–SE oriented systems of thrust-folded terranes (Funiciello *et al.* 1981).

Detailed mapping of the frontal region of the Gran Sasso chain (Ghisetti & Vezzani 1986a,b) leads to recognition of an imbricate stack defined by eight major thrust faults (numbered from T_1 to T_8 in Fig. 2) which bound eight thrust sheets, whose stratigraphic assemblages can be partially differentiated. The thrust sheets are deformed internally either by cataclasis or by folding, but the intensity of deformation increases markedly towards the thrust faults.

The aim of this paper is to highlight the structural features of the thrust faults in order to derive information on the progressive deformation history and on the mechanisms of thrust sheet emplacement associated with the Upper Miocene–Lower Pliocene thrusting event.

CHARACTERS OF THE THRUST SYSTEM

The thrust faults which have been identified in the northeastern portion of the Gran Sasso chain cause the imbrication of the thrust sheets numbered from 1 to 8 in

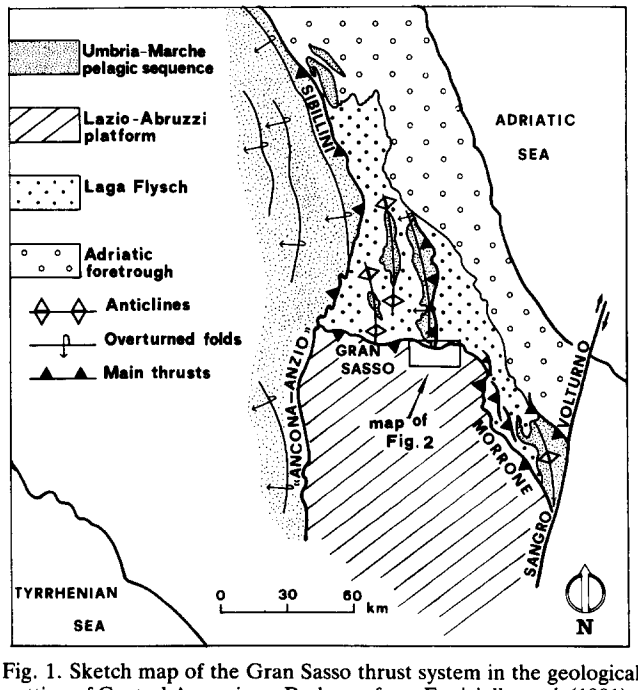

Fig. 1. Sketch map of the Gran Sasso thrust system in the geological setting of Central Apennines. Redrawn from Funiciello *et al.* (1981).

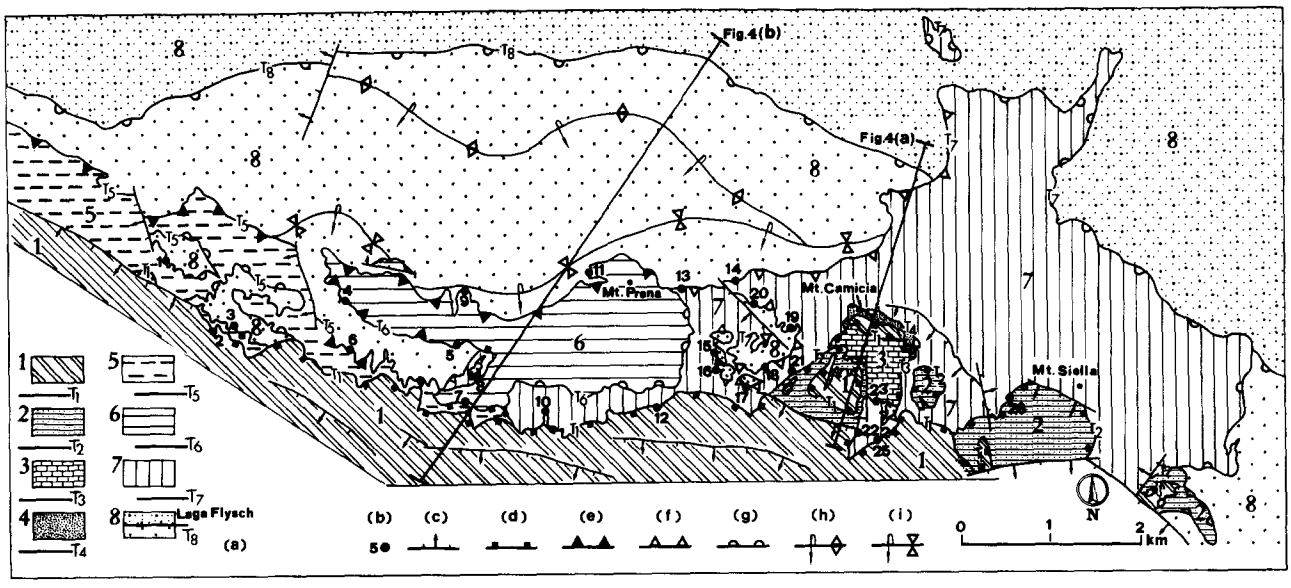

Fig. 2. Simplified map of the study area. (a) Thrust sheets ('units') (1–8) and basal thrusts (T_1–T_8) are numbered in order of decreasing elevation in the tectonic imbricate stack, stratigraphic boundaries within each unit are not indicated (see Fig. 3); (b) sites of structural sampling; (c) normal faults; (d); (e); (f); (g) thrust faults, with barbs on the overthrust side, the different symbols used for barbs indicate: (d) cataclastic thrust faults; (e) thrust faults truncating folds developed in the footwall units; (f) thrust faults truncating folds developed in the hangingwall and footwall units and bordered by foliated fault rocks; (g) thrust faults with weak or undetectable deformations; (h) axial trace of overturned anticlines; and (i) axial trace of overturned synclines.

Fig. 2, which can be mapped as distinct 'units' on the basis of differences in their litho-stratigraphic assemblages and facies. However, numerous similarities in the stratigraphic sequences within these units indicate that they are portions of adjacent sedimentary domains, originally located in an interfingering area between the Latium–Abruzzi carbonate platform and the Umbria–Marche pelagic basin (Parotto & Praturlon 1975).

Description of the tectonic units

The stratigraphic sequence which is exposed in each thrust sheet is shown in Fig. 3; for the sake of simplicity the stratigraphic boundaries within each unit are not shown on Fig. 2. The main features of each unit are briefly summarized below, starting with the lowermost unit in the imbricate stack and proceeding in order of ascending tectonic elevation.

Unit 8 consists of a pelagic sequence developed from Middle Lias to Eocene–Oligocene times. The sequence starts with micritic cherty limestones of the Corniola Formation (Middle Lias) grading upwards to calcareous marls of the Verde Ammonitico Formation (late Lias-Dogger). The sequence continues with a calcareous-turbiditic formation (Calcareniti a Entrochi of Dogger–early Cretaceous age), overlain by micritic cherty limestones of the Maiolica Formation (early Cretaceous), which in their turn are covered by calcareous marls and cherty limestones of the Scaglia Formation (Upper Cretaceous–Oligocene). This pelagic sequence is characterized by strong detrital supply, mostly within the Corniola, Maiolica and Scaglia formations. The pelagic sequence evolves upwards (Fig. 3) into calcarenites, marls and clays of Middle Eocene and Miocene age (Glauconitic calcarenites and Cerrogna marls) and ends with the Upper Miocene–Lower Pliocene Laga Flysch.

The sequence of *unit 7* starts with Middle (?)–late Triassic grey dolomites with thin interlayers of bituminous shales, grading upwards to Lower Liassic dolomitic limestones. The overlying formations (Corniola, Verde Ammonitico, Calcareniti a Entrochi, Maiolica and Scaglia) indicate persisting pelagic conditions from Middle Lias to early Eocene times. Calcirudites of early Eocene age and glauconitic calcarenites of Middle Eocene–Lower Miocene age are the uppermost formations in the sequence.

The bulk of *unit 6* consists of massive early Liassic dolomites, grading upwards to well-bedded white dolomites. In the mapped area, the sequence of *unit 5* consists only of early Liassic stromatolitic dolomites, but the overlying formations (Corniola, Verde Ammonitico and Maiolica) crop out in an adjacent zone to the west.

The small thrust sheet of *unit 4* consists exclusively of Middle Lias cherty limestones (Corniola Formation) which cannot be ascribed to any of the recognized sequences.

Units 2 and 3 are very similar (Fig. 3); they are made up of early Liassic dolomites overlain by a pelagic sequence which developed from Middle Lias to Dogger times (Corniola and Verde Ammonitico). The overlying sediments are calcarenites of Dogger-early Cretaceous age (Calcareniti a Entrochi).

The prevailingly pelagic sequence of *unit 1* starts with cherty limestones of the Corniola Formation (Middle Lias) and terminates with the late Cretaceous–early Eocene Scaglia Formation. This sequence is characterized by two thick clastic formations: the first (Cal-

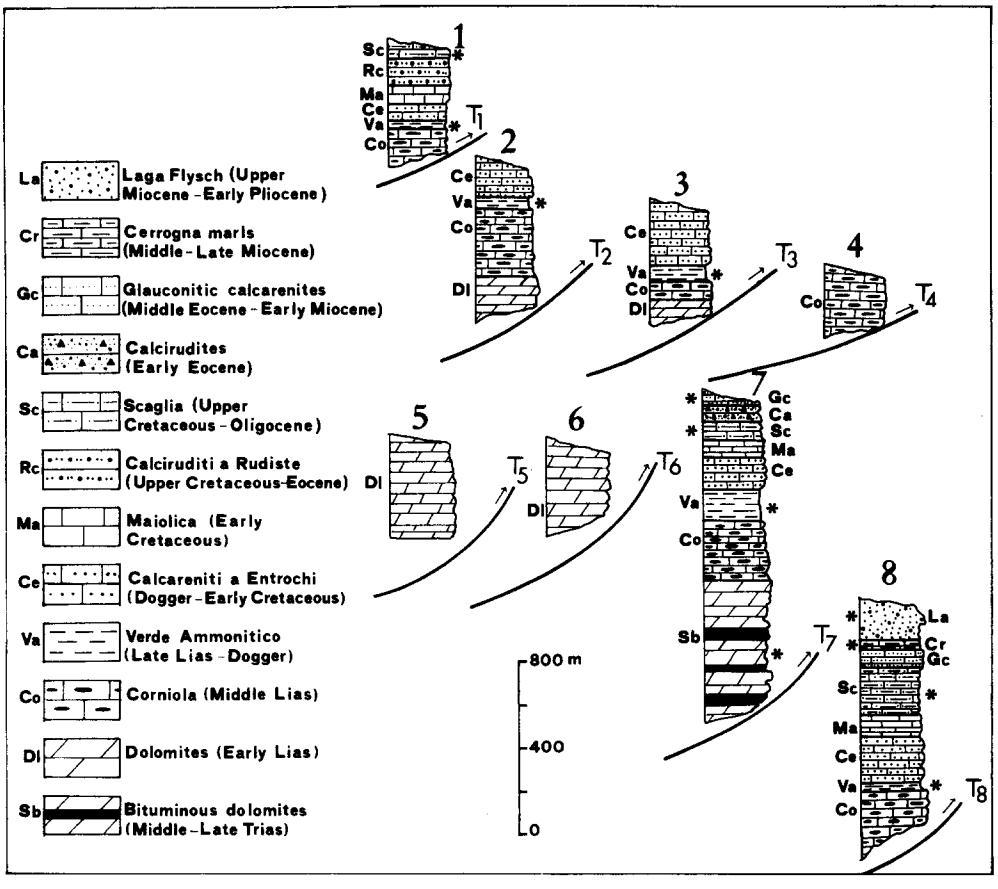

Fig. 3. Stratigraphic columns of the exposed sequence in each of the thrust sheets of Fig. 2. For a description of lithologies see text. Asterisks indicate low-competence beds.

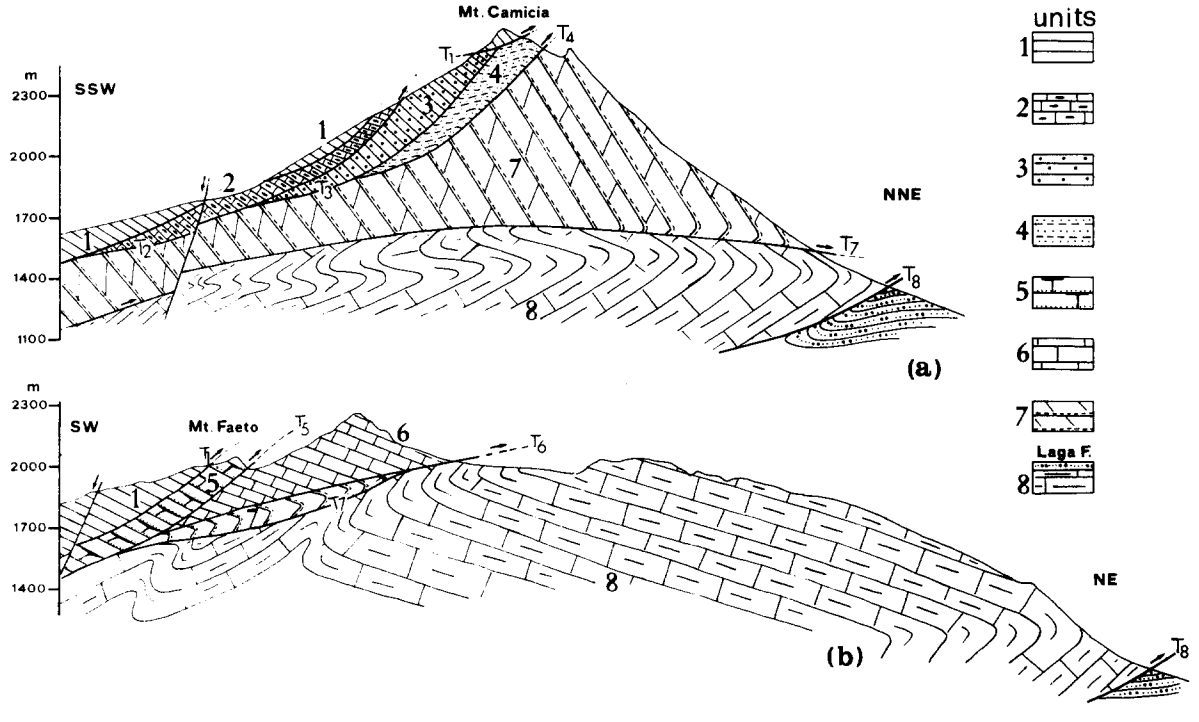

Fig. 4. Cross-sections (trace in Fig. 2) showing the mutual relationships between the thrust sheets in the imbricate stack. Symbols used for each undifferentiated unit are oriented according to bedding attitude.

careniti a Entrochi of Dogger–early Cretaceous age) occurs between the Verde Ammonitico and Maiolica formations and the second (Calciruditi a Rudiste of Upper Cretaceous–Eocene age) is interlayered between the Maiolica and Scaglia formations.

Geometrical setting of the imbricate thrust system

Each of the units described constitutes a thrust sheet bounded by a basal thrust fault (Fig. 2). Due to the wedge shape of the thrust sheets, no existing single section shows a complete sequence of all the stacked units, but mutual relationships in different portions of the chain suggest that elevation in the tectonic stack increases from unit 8 to unit 1 (Fig. 4). The sections show that imbrication in the tectonic stack results in the exposure of the lowermost units (7 and 8) along the northern scarp of the mountain range. The uppermost units of the tectonic pile occur in a step-like fashion on the gentle southern flank of the chain (Figs. 2 and 4), where they are truncated by normal faults of Pleistocene–Holocene age (Demangeot 1965). Units 1–6 occur in E–W trending, N-dipping monoclines, which are constantly truncated up-section by the thrust faults. The lowermost units 7 and 8 are broadly deformed by systems of E–W-trending folds (Fig. 4a & b).

All the thrust faults possess a fairly constant E–W strike and generally dip 15–30° towards the south; the T_7 and T_8 thrust faults are characterized by large-scale undulations. The geometrical relationships among the different thrust faults are shown in Fig. 4(a) & (b) and described below.

T_1 intersects all the other thrust faults, thereby emplacing unit 1 on units 2, 5, 7 and 8 along the southern flank of the chain. A small klippe of unit 1 overrides units 3 and 4 at Mt. Camicia (Figs. 2 and 4a). T_2 cuts T_3 and T_7, with resulting overthrusting of unit 2 onto units 3, 7 and 8 between Mt. Camicia and Mt. Siella (Figs. 2 and 4). T_3 and T_4 are minor tectonic contacts that emplace the small klippen of units 3 and 4 on unit 7 in the Mt. Camicia area. T_5 develops in the western sector of the mapped area, where unit 5 overlies units 6 and 8. T_6 overthrusts the klippe of unit 6 onto units 7 and 8. T_7 has emplaced unit 7 onto unit 8; it has a convex surface (Fig. 4a) and is repeatedly intersected by the erosion surface, thus revealing unit 8 in several tectonic windows along the southern flank of the chain (Fig. 2). T_8 is the frontal thrust of the imbricate stack (Fig. 1). It is the only one to cut across the same unit (8), with the thrusting of Middle–Upper Miocene calcareous marls on the Upper Miocene–early Pliocene sediments of the Laga Flysch (Figs. 2 and 4).

DEFORMATION FEATURES OF THE THRUST FAULTS

Description of fabrics in the different thrust faults

Displacement along the major thrust faults is associated with different deformations, as described below.

The T_1, T_2 and T_3 thrust faults show remarkably similar deformation features; they are bordered by breccia and gouge zones from a few metres to as much as 50 m thick. In the case of thrust fault T_5 the same features occur only where unit 5 directly overrides unit 6 (near to site 7 in Fig. 2). The cataclastic belts seem to be thickest where faulting occurs between dolomites, but cataclasis causes intense disruption of calcareous rocks as well. Detailed observations at sites 2, 10, 23 and 25 (Fig. 2) indicate that the cataclastic thrust boundaries develop by the linking of tightly clustered sets of sub-parallel shears, which juxtapose brecciated rocks of different grain size (from ultra-fine gouge to coarse fragments) and degree of cementation. Alternating levels of different grain size, separated by thin shear zones where fine-grained material is concentrated, define banding in a direction parallel to movement planes. Grooved cemented planes are frequently observed; they separate differently disrupted domains, crossed by an array of fractures and tension gashes. The density of interconnected fractures decreases markedly away from the thrust zones. The thin sections of some samples (sites 2, 10, 12, 25 in Fig. 2) contain coarse-twinned calcite aggregates and heavily fractured cherty grains which are embedded in an ultrafine cataclastic matrix. Fractures in the coarser grains do not propagate into the surrounding matrix. Calcite veins and a few stylolitic joints also occur in these rocks.

The T_5 and T_6 thrust faults show different deformation features at those sites where units 5 and 6 are overthrust directly on unit 8 (Fig. 2). The dolomites of the hangingwall units are crossed by an array of spaced fractures (sites 4, 5, 6 in Fig. 2), but the thrust surfaces are extremely sharp and they truncate folds that developed in the footwall rocks, close to the cutoff of unit 8 against T_5 and T_6 (Fig. 5). The sequence of unit 8 is deformed by a *Z*-shaped, chevron-like system of flexural-slip folds, exposed along the northern scarp of the chain for about 7 km (Figs. 2 and 5). The folds are characterized by E–W-trending axial planes, gently dipping to the south. The *Z*-shape is defined by a syncline–anticline system, linked by an upright monoclinal limb. The overturned limb of the syncline is truncated at different levels by T_5 and T_6 (Fig. 5a & b), whereas the overturned anticlinal limb is overthrust on the Laga Flysch along the T_8 fault. The geometry of the fold system, as observed in the footwall of the T_5 and T_6 thrust faults (Fig. 5a & b) suggests a progressive rotation of bedding and axial planes towards the thrust boundaries; amounts of rotation are larger underneath T_6.

Increasingly large deformations are observed in the case of T_7, whose fault surface cuts across folds developed in both the hangingwall and footwall units (Fig. 5c & d). In the footwall of T_7 the *Z*-shaped fold system which deforms unit 8 is tightened resulting in a recumbent fold (Fig. 5c). Development of minor folds in the footwall of T_7 is also apparent in tectonic windows which reveal unit 8 on the southern flank of the chain (Figs. 2 and 5e). The rotation of fold axial planes towards the T_7 thrust fault can again be measured on the outcrop

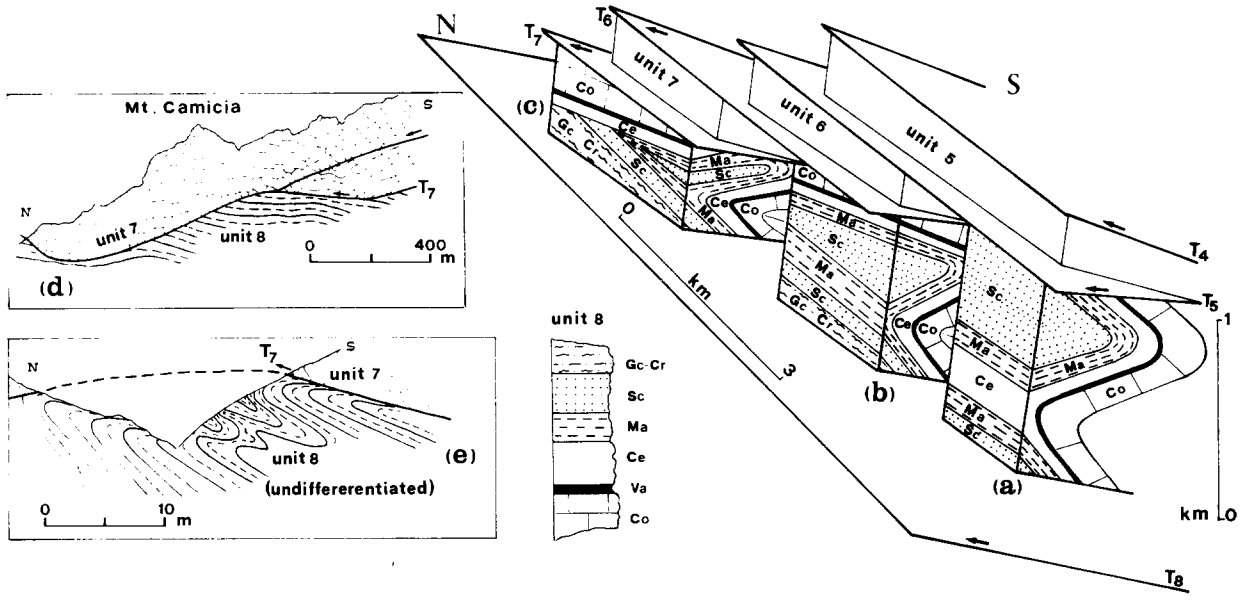

Fig. 5. (a)–(c) Progressive tightening of the Z-shaped fold system in unit 8, by increasing amounts of rotation of bedding and axial planes in the footwall of thrust faults T_5, T_6 and T_7. The stratigraphic sequence of unit 8 is indicated in the column, where formations are labelled according to Fig. 3. Bedding in units 5, 6 and 7 is not shown; (d) details on bedding in unit 7, in the hangingwall of the T_7 thrust fault; and (e) small-scale folds developed in the footwall of the T_7 thrust, as detectable in tectonic windows located on the southern flank of the chain (Fig. 2).

scale (Fig. 6). The most interesting deformation feature peculiar to T_7 is the development at the thrust boundary of small-scale duplexes (1–5 m thick) where lenses of cataclastic rocks are surrounded by foliated fault rocks (Fig. 7). The best documented examples have been observed in the tectonic windows of unit 8 underneath unit 7 (sites 8, 16, 17, 18, 19 in Fig. 2). Duplexes tighten and enlarge along the thrust boundary due to undulations in the floor and roof thrusts, with sharp contact of the two overlapping units where the two planes rejoin. The imbricate stack within the duplex is defined by minor thrusts at varying angles to the main boundaries. Lens-shaped tectonic slices have been detached from both the underlying and overlying units, with a complex sandwiching of contrasting lithologies. The largest lenses which were derived from dolomites mainly show cataclasis, whereas lenses of cherty limestones (Corniola Formation) and calcareous marls (Verde Ammonitico Formation) show cataclasis and pressure solution. Elongated lenses tend to be aligned parallel to the thrusting direction. The largest rigid slices are tectonically interfingered with the foliated fault rocks (Fig. 7), whose fabrics will be described in detail in the next section. Bedding cannot be recognized in the duplexes, but, outside the thrust zone, layers rotate into parallelism with the movement planes, probably because of the folding mechanism described above (Fig. 6).

Classification of the thrust faults

On the basis of the described deformation features, the principal thrust faults mapped in Fig. 2 may be

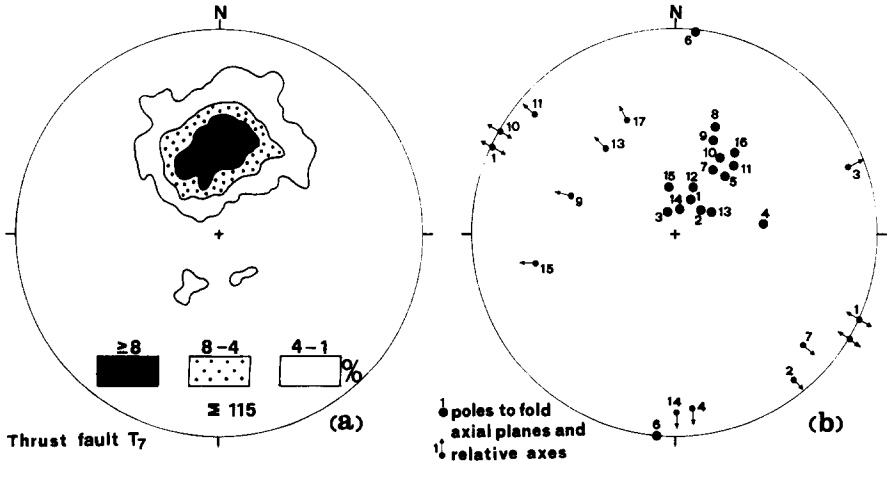

Fig. 6. Relationships between attitude of the thrust surface T_7 and small-scale folds developed in unit 8, immediately adjacent to the thrust boundary. (a) Density plot of the T_7 thrust surface, measured at different localities; and (b) stereonet of fold attitude in unit 8 at sites 16–19 in Fig. 2 (Schmidt projection, lower hemisphere); for field relationships see Fig. 5(e).

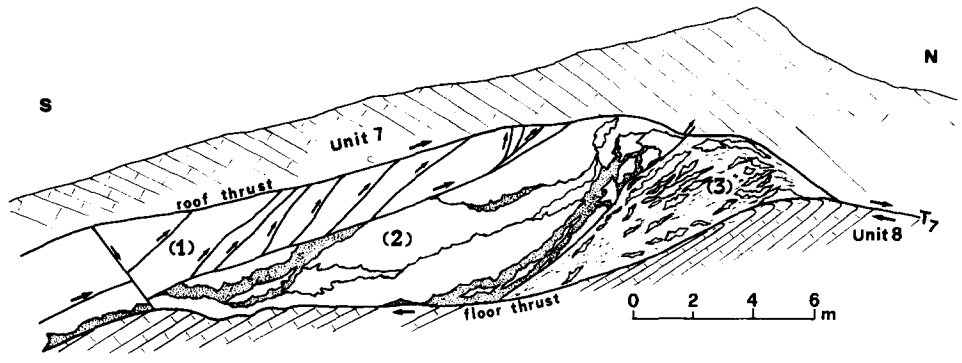

Fig. 7. Sketch from photograph of one duplex developed at the boundary between units 7 and 8 (site 17 in Fig. 2). The thrust faults, splaying at different angle from the floor thrust, separate domains with different deformation features. (1) Imbricate stack of crushed dolomitic lenses derived from unit 7; (2) cataclastic flow and indentation of calcareous units sliding within foliated fault rocks (dotted); and (3) lenticular segregation by flow of marly-calcareous levels (Verde Ammonitico Formation).

grouped as follows: (1) thrust faults marked by thick belts of incoherent gouges and breccia zones (T_1, T_2, T_3 and, locally, T_5); (2) thrust faults characterized by a sharp, brittle contact, truncating flexural-slip folds that had developed in the footwall units (T_5, T_6); and (3) thrust faults cutting across folds developed in both the footwall and hangingwall units and bordered by foliated cataclasites (T_7). The subdivision into three groups takes into account the dominant features only; deformation fabrics may actually vary along the same thrust surface (e.g. T_5) or in places may not be detectable due either to very low amounts of deformation (e.g. T_4) or to poor exposure. T_8 has not been included in any of the three groups due to poor exposure, although deformation features at its boundary are similar to those observed for T_7, as far as folding in the hangingwall and footwall units is concerned (Figs. 2 and 4). The variation in deformation fabrics that occurs along the thrust faults is mapped in Fig. 2 by means of different symbols.

STRUCTURAL FEATURES OF THE FOLIATED FAULT ROCKS

The foliated fault rocks associated with the T_7 thrust fault have been studied in some detail, due to their peculiar fabric, and for the information they can provide regarding deformation mechanisms.

Mesoscopic structures of the foliated fault rocks

The foliated fault rocks occur in bands a few centimetres to 1 m thick. These rocks seem to originate mainly in the thinly-bedded bituminous dolomites of unit 7 and in the cherty limestones and calcareous marls (Corniola and Verde Ammonitico formations) of unit 8 (Fig. 3), where they are brought into contact within the small-scale duplexes (Fig. 7) associated with the T_7 thrust fault (e.g. sites 8, 15, 16, 17, 18, 19, 20 in Fig. 2).

Fabric in the fault rocks is defined by three main families of surfaces, unevenly distributed in adjacent domains (Figs. 8 and 9). Planes defining the macroscopic foliation resemble spaced anastomosing cleavage (Powell 1979, Borradaile *et al.* 1982, Engelder & Marshak 1985), separating lens-shaped microlithons (Fig. 8a). The largest calcareous microlithons embedded in a clayey matrix show internal cataclasis and stylolitic indentation where they are forced into contact. Cleavage planes converge asymptotically and rotate into flat microshears which are parallel to the thrust fault T_7 (Fig. 8b & c). Lenticular partitioning and elongation of microlithons towards the thrust direction is accomplished by a system of synthetic *R*-type Riedel shears (Morgenstern & Tchalenko 1967, Gamond & Giraud 1982). The geometrical relationships between the three systems of planes indicated as *S* (cleavage), *C* (shear) and *R* (Riedel), respectively, and their attitude relative to the thrust fault T_7 are shown in Fig. 9. *S* planes generally intersect the *C* surfaces at angles of about 30–40°, but in the most deformed rocks they rotate towards the *C* surfaces and both make a fairly low angle to the main thrust fault (Figs. 8c and 9). Where fabric develops in clay-rich domains (e.g. Verde Ammonitico Formation) fault rocks are deformed by a complex system of disharmonic folds, truncated by the *C* shears (Fig. 10). Some of these folds seem to be produced by local flow perturbations (e.g. Lister & Williams 1983), due to the imbrication of rigid microlithons. In most of the examples observed, however, asymmetry of folding is consistent with the sense of shearing on the *C* planes, and field observations provide examples of different stages of progressive rotation of steeply inclined axial surfaces towards parallelism with the *C* shears (Fig. 10). Fold axes rotate towards the shear direction as well.

Microscopic features of the foliated fault rocks

Thin-sections of the fault rocks have been cut approximately parallel to the *XZ* and *YZ* planes, where the *XY* plane is defined by the foliation surfaces *S*. The lithology of the sampled rocks includes pelletal limestones with a micritic cement, calcareous mudstones with chert, bioclastic limestones rich in cherty particles, sparry calcite grains and crinoidal fragments (Corniola and Verde Ammonitico formations). Ultrafine micrites with varying amounts of brown amorphous material could be ascribed to the bituminous dolomites of unit 7.

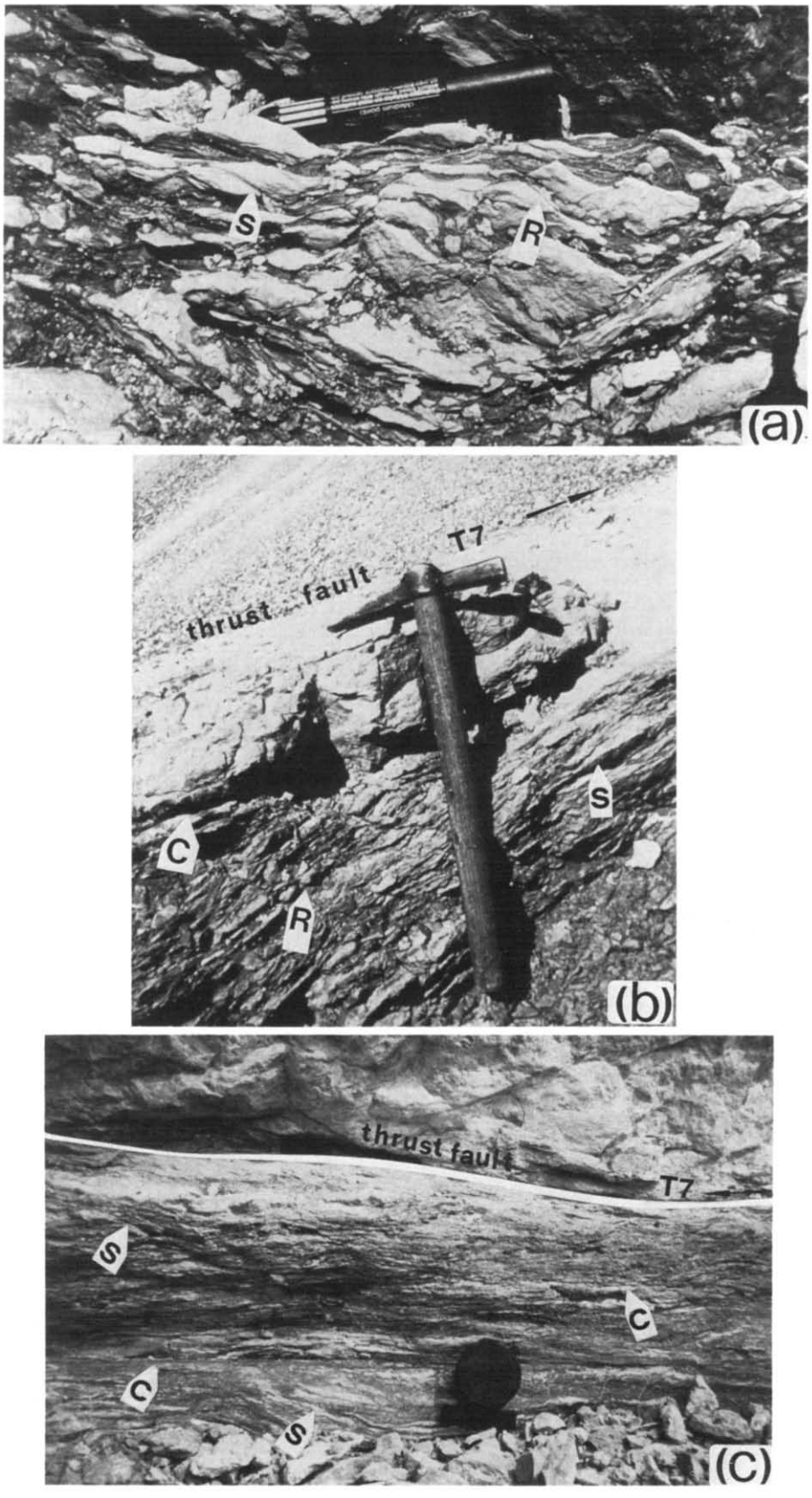

Fig. 8. Examples of fabric in the foliated fault rocks. (a) Development of anastomosing cleavage surfaces, separating lens-shaped microlithons, note stylolitic indentation at impingement points and Riedel fractures. *R*, length of pen = 12 cm. (b) Cleavage surfaces *S* intersecting the main thrust fault T_7 at an angle of about 30°, note again development of Riedel fractures *R*, length of hammer = 45 cm. (c) Example of highly deformed fault rocks, characterized by cleavage surfaces *S*, and *C* shears both sub-parallel to the main thrust fault T_7, diameter of lens cap = 5 cm.

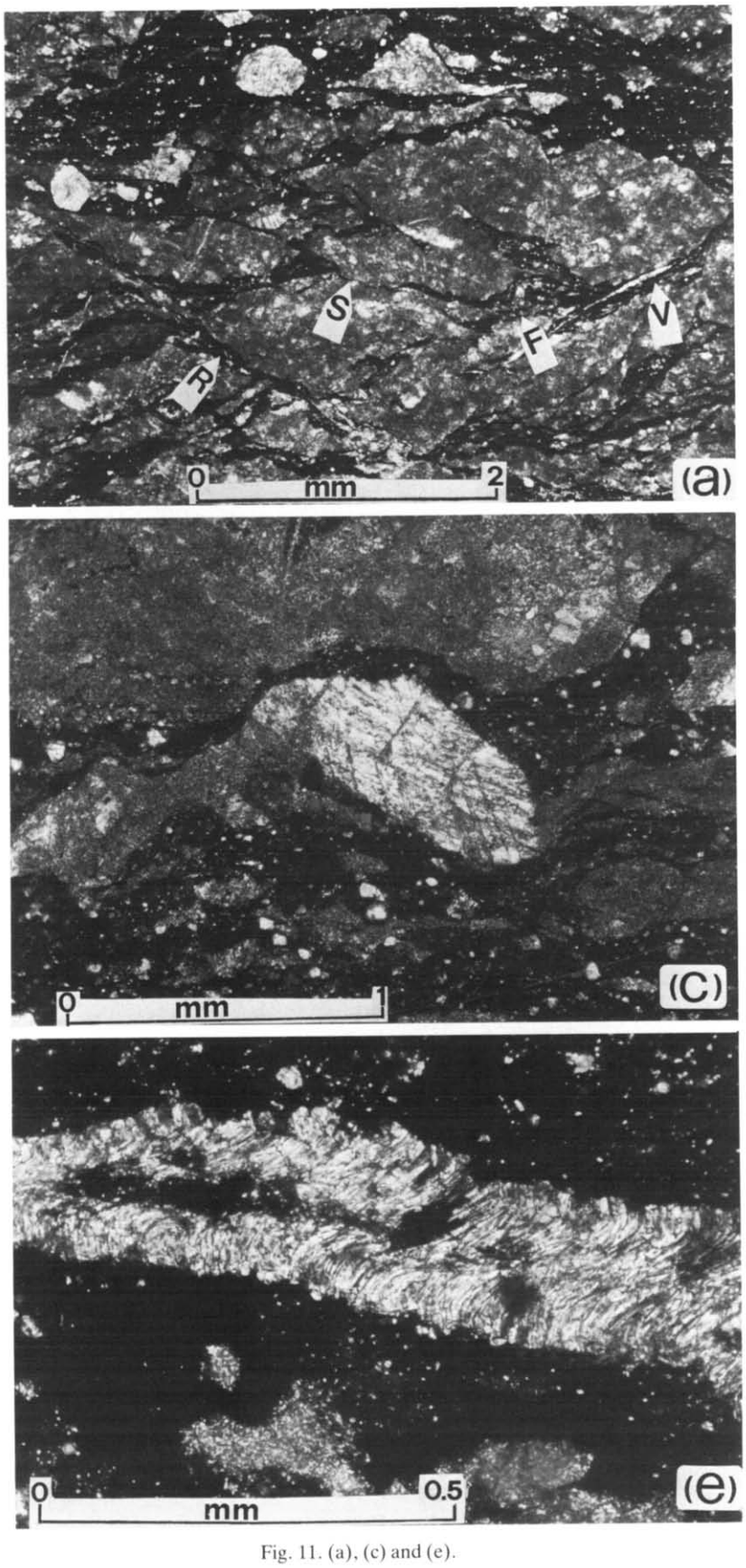

Fig. 11. (a), (c) and (e).

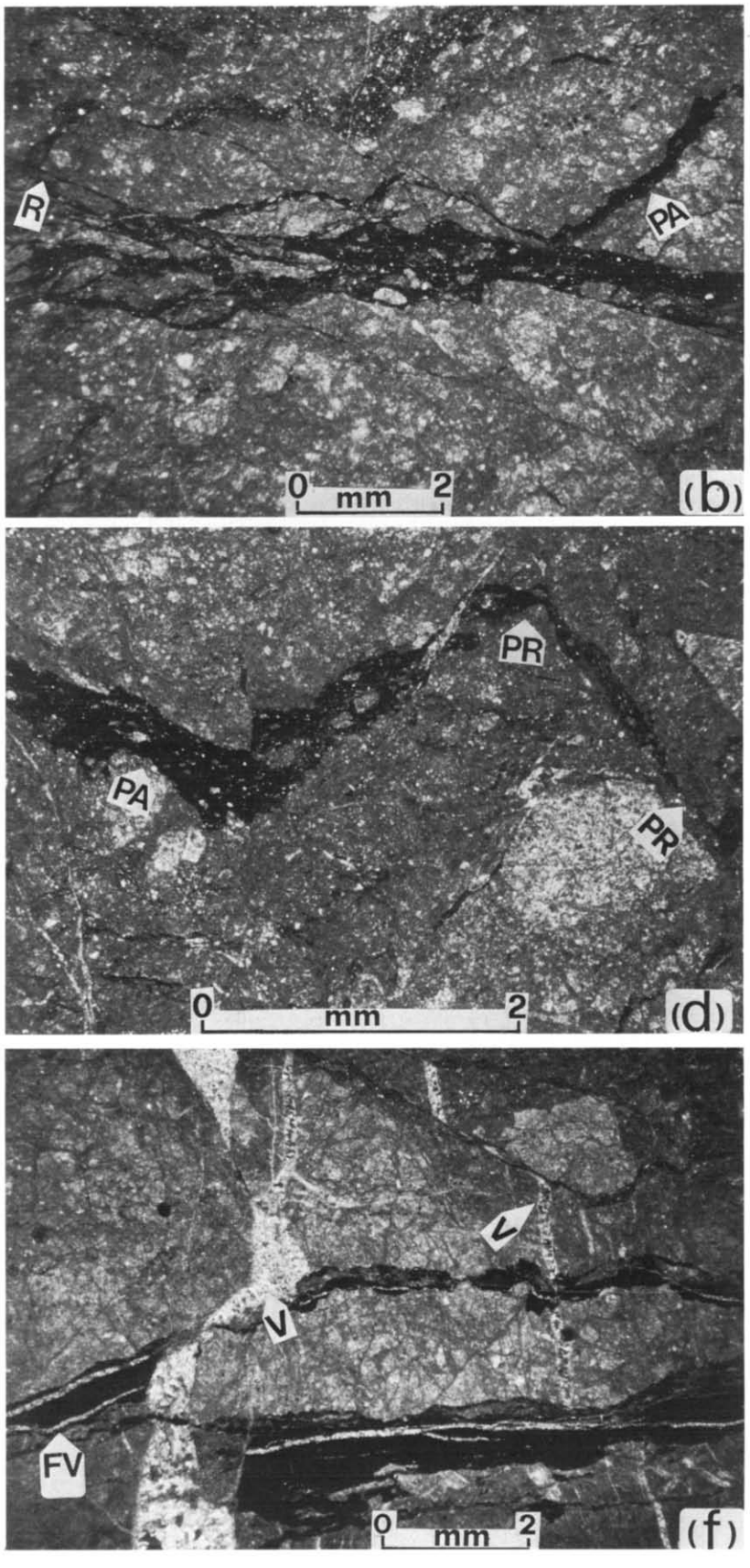

Fig. 11 *continued*. Photomicrographs of foliated fault rocks. (a) Propagation of coalescent microshears in a crushed rock, with local development of stylolitic indentation (*S*) at impingement points and calcite veins (*V*) in the intergranular space, note local microfolding (*F*) by flow perturbation. (b) Development of a through-going microshear, characterized by microlithons flowing in a dark matrix, note the shape alignment, the development of Riedel (*R*) fractures and the progressive detachment of microlithons, creating 'pull-apart' (*PA*) zones. (c) Rotation of a sparry calcite grain within a microshear. (d) 'Pull-apart' (PA) and pressure-ridge (*PR*) morphology created by relative sliding of irregular-shaped microlithons within a microshear. (e) Enlargement of a fibrous vein developed within a microshear. (f) Calcite veins (*V*) at high angle to the microshears, undergoing pressure solution, shearing or crushing, and fibrous veins (*FV*) parallel to the microshears.

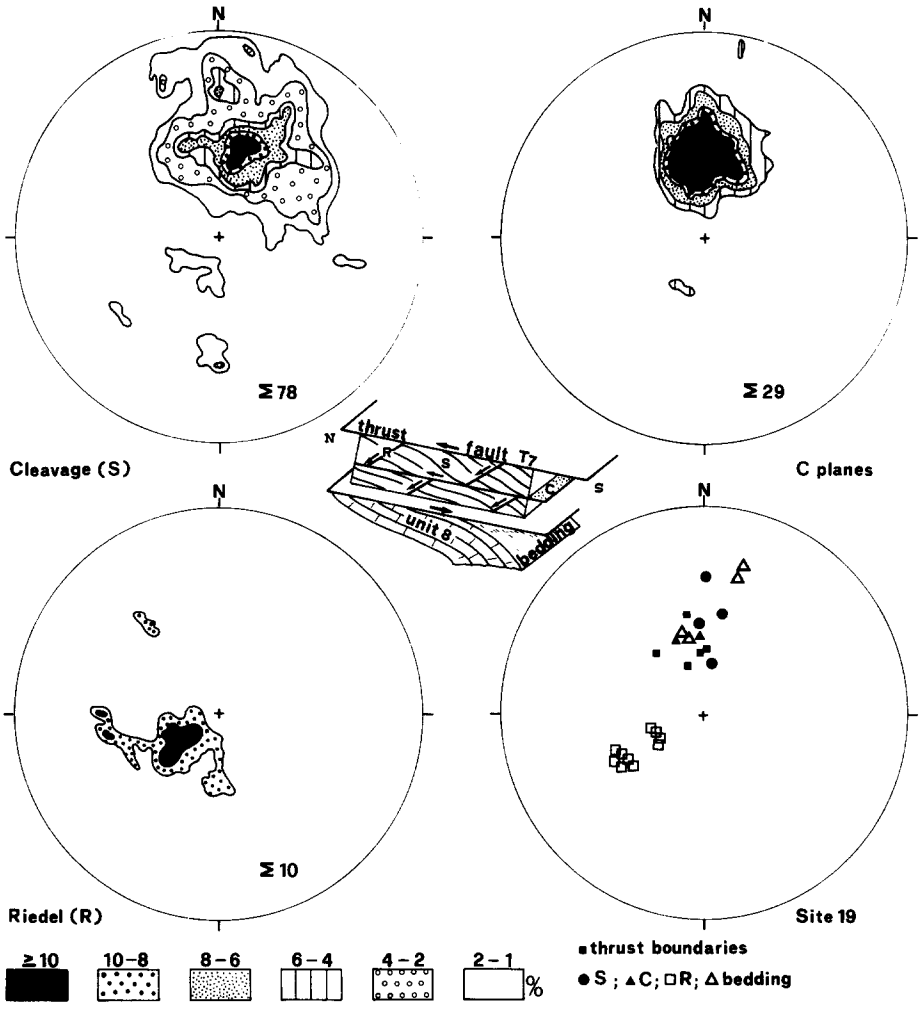

Fig. 9. Density plots (Schmidt projection, lower hemisphere) illustrating the relationships among cleavage *S*, *C* shears and Riedel *R*-type fractures in the foliated fault rocks (data collected at sites 8 and 15–20 in Fig. 2). See Fig. 6(a) for attitude of the thrust surface T_7. The geometrical relationships among *S*, *C* and *R* surfaces are sketched, and shown for the sampling site 19.

All the samples show through-going interconnected fractures propagating across internally crushed grains, and in some sections (e.g. Fig. 11a) preferential shape alignment seems to be produced by intergranular motion of individual elongate fragments within the gouge, with solution pitting at grain-to-grain indentations (Fig. 11a). An increasing amount of deformation seems to be testified by progressive reduction in grain size, further rotation of the largest grains, and production of ultrafine gouge in unevenly spaced, coalescent zones (Fig. 11b). These zones seem to define the microscopic cleavage and appear as dark-coloured strips of different width, where detached angular fragments are floating and flowing around larger microlithons (Fig. 11a & b). The dark material infilling the microfractures could be interpreted as either ultra-fine gouge or as derived from the bituminous dolomites. Shearing along these discrete zones is indicated by different features: rotation of grains within the ultrafine matrix (Fig. 11c), local microfolding around the largest grains probably due to flow perturbations (Fig. 11a), and development of a pull-apart 'pressure-ridge' morphology created by relative slip along the irregular shearing surfaces (Fig. 11b & d). The impingement points between microlithons are stylolitic, whereas the pull-apart regions are infilled with gouge and fibrous calcite veins (Fig. 11a, e & f). Orientation of the fibres varies as a function of the displacement vector between adjacent microlithons. Another set of veins infilled with equant, sometimes twinned, sparry calcite intersects the microshears at a high angle (Fig. 11f). At the intersection, these veins may undergo pressure solution, cataclastic crushing, buckling or progressive reorientation by shear. Planes of discrete *R*-type Riedel fractures cause further segmentation of the clastic grains (Fig. 11a & b), thus contributing to the process of textural layering by elongation of grains in the cleavage zones. The three-dimensional shape of microlithons indicates elongation in both the *X* and *Y* directions and flattening in the *XY* plane.

DEFORMATION MECHANISMS IN THE THRUST ZONES

Field observations indicate that cataclastic crushing, folding and cleavage development are associated with thrust sheet emplacement, but their relative importance in the different thrust faults of the imbricate stack seems to vary.

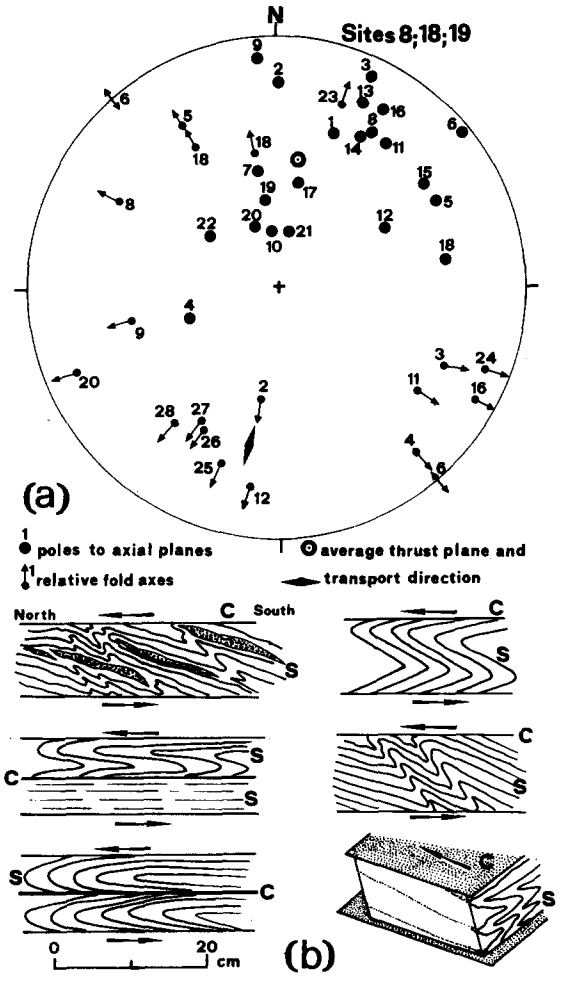

Fig. 10. (a) Poles to axial planes, and fold axes (Schmidt projection, lower hemisphere) of the small-scale folds developed in the foliated fault rocks at sites 8, 18, 19 in Fig. 2. The stereonet shows the clustering of axial planes around the average thrust plane T_7, and the variable orientation of fold axes to the thrust direction. (b) Sketches of field relationships (redrawn from photographs) between folded *S* surfaces and *C* shears in the foliated fault rocks. Note the different style of folding of the *S* surfaces and the variable rotation towards the *C* planes. All the drawings possess the same orientation, *C* surfaces have been drawn horizontal, but they actually dip of about 20–40° to the south (Fig. 9).

The basal thrust faults of the uppermost units (T_1, T_2, T_3 and, locally, T_5) are marked by thick belts of incoherent gouges and cataclasites. Although a principal thrust plane can be mapped, movements are accommodated by a complex system of interconnected shears, with incipient mechanisms of cataclastic flow along subtly distributed shear zones. The cataclastic fault zones seem to have grown in thickness by intense crushing in both the hangingwall and footwall units, with consequent development of an array of linked microcracks. The growth in thickness of the breccia zones could be attributed to strain-hardening effects along the cemented movement planes. Mandl *et al.* (1977) suggest this effect can be related to the segregation of the finest grains in the shear zones, due to dilatancy during cataclastic flow (see also Blenkinsop & Rutter 1986). The occurrence of this process seems to be suggested by the banding observed in the breccia zones, which is defined by alternating layers of different grain size.

Deformation features of the fault zones T_5, T_6 and T_7 indicate that emplacement of units 5, 6 and 7 on unit 8 follows an early phase of shear-induced folding (e.g. Ramsay *et al.* 1983) in units 7 and 8. Folding seems to accommodate compression prior to the final propagation of the thrust faults. Deformation mechanisms change at those thrust boundaries (like T_7) where fold limbs and axial planes have been brought parallel to the thrust planes, with the development of foliated cataclastic fault rocks. The field setting indicates that the fault rocks result from localized shear motion within small-scale duplexes, where contrasting lithologies are juxtaposed by shear planes parallel to the principal thrust fault.

Rocks with similar fabrics have been described by Koopman (1983) and Lavecchia (1985) in the Sibillini thrust front (Fig. 1). According to Koopman (1983), fabric in the fault rocks originated by pressure-solution cleavage, subsequently truncated by shears equivalent to the *C* planes of this paper, and by Riedel shears of the *R'* type. The dominant role of cataclasis in producing flow and foliation by mechanisms of rigid-body rotation of particles, flattening and segregation of mineral components, with the development of Riedel shears, has been emphasized by Chester *et al.* (1985) in relation to cataclasites in the San Andreas fault system.

In the study area, microscopic observations suggest that fabric in the fault rocks originates from initial crushing, consequent reduction in grain size and the onset of cataclastic flow of the aggregate as a whole. Increasing deformation leads to the through-going development of microshears along which microlithons slip in relative motion. The irregular shape of microlithons acted as a geometrical obstacle which was overcome by the production of increasing amounts of gouge at the microlithon boundaries, by flow of the finer matrix around larger grains and by pressure-solution slip (Elliott 1976, Marshak *et al.* 1982, Gamond 1983) in the locked margins, as indicated by the presence of fibrous veins associated with stylolitic indentation along the cleavage surfaces. The observed presence of sparry calcite veins deformed at the cleavage intersection suggests that these veins formed at an early stage of fabric development and that they were subsequently subjected to different deformation conditions when the onset of pressure-solution slip caused progressive shear along the cleavage surfaces. The pervasive development of the microscopic fabric is testified on the mesoscopic scale by the *S* planes, which are truncated by both the *C* and *R* surfaces. Progressive rotation of the fabric towards the thrust direction seems to favour easy-slip conditions during the thrusting event.

CONCLUSIONS

The Gran Sasso thrust belt is made up by a system of imbricate thrust sheets emplaced at crustal levels where brittle conditions dominate. The almost complete lack of intracrystalline deformation indicates low temperatures (<200–300°C) and pressures (equivalent to depths

of <5–10 km) for all the thrust faults (see e.g. Engelder & Marshak 1985). Mechanisms of motion vary in the different thrust zones, depending on their elevation in the tectonic stack, and they may vary along the same thrust fault in connection with changes in the hanging-wall and footwall lithologies. The occurrence of prevailing cataclasis, or shear-induced folding, or cataclastic flow with pressure-solution slip in the foliated fault rocks can be accounted for by the interplay of the following factors: (1) lithologic changes and mechanical contrasts in the units which have been brought into contact by the thrust faults; and (2) larger amounts of deformation in the deepest portions of the imbricate stack.

The stratigraphic sequence of units 7 and 8 (Fig. 3) consists of a multilayer with repeated occurrence of low-competence beds, in contrast with the stratigraphic sequence of the overlying units (from 1 to 6), where massive calcareous and dolomitic beds are dominant. These mechanical contrasts could explain why units 7 and 8 undergo shear-induced folding prior to the propagation of the brittle thrust faults T_5, T_6, T_7 and T_8, whereas units 1, 2, 3, 4, 5 and 6 maintain a monoclinal setting on a regional scale. The upper units are truncated up-section by cataclastic fault zones cutting across bedding at a uniform angle.

In the deepest unit of the stack (unit 8) the geometry of the *Z*-shaped fold system is progressively modified by rotation of axial planes and bedding towards the thrust faults. The increasing amount of rotation observed in the footwall of the thrust faults T_5, T_6 and T_7, respectively (Fig. 5a, b & c) is consistent with an amount of horizontal displacement that increases progressively from the uppermost to the lowermost thrust sheets in the imbricate stack (Ghisetti & Vezzani 1986b). The thrust fault T_7 is characterized by intense deformations, with development of distinctive foliated cataclasites. The fault rocks appear to have formed only where bedding has been reoriented at a low angle to the thrust zone, thus suggesting that bedding discontinuities are the site of preferential slip at an early stage. Later development of a textural fabric by mechanisms of cataclasis and pressure-solution slip, combined with pervasive shearing, causes a final transposition of the original layering. Field data suggest that the foliated fault rocks prevalently occur where the T_7 fault overthrusts the bituminous dolomites of unit 7 on the calcareous marls and cherty limestones (Verde Ammonitico and Corniola formations) of unit 8, thus indicating that lithology exerts an important control on fabric development.

Acknowledgements—This work was carried out as part of the research program supported by C.N.R. grant No. 20120401.85. The author is grateful to L. Vezzani for discussions in the field and for constructive criticism. Finally, careful editing by D. J. Sanderson and comments from two anonymous reviewers resulted in considerable improvements to the text.

REFERENCES

Blenkinsop, T. G. & Rutter, E. H. 1986. Cataclastic deformation of quartzite in the Moine thrust zone. *J. Struct. Geol.* **8**, 669–681.

Borradaile, G. J., Bayly, M. B. & Powell, C. McA. 1982. *Atlas of Deformational and Metamorphic Rock Fabrics*. Springer Verlag, Berlin.

Chester, F. M., Friedman, M. & Logan, J. M. 1985. Foliated cataclasites. *Tectonophysics* **111**, 139–146.

Demangeot, J. 1965. *Géomorphologie des Abruzzes Adriatiques*. Mem. et Doc. C.N.R.S.

Elliott, D. 1976. The energy balance and deformation mechanisms of thrust sheets. *Phil. Trans. R. Soc. Lond.* **A 283**, 289–312.

Engelder, T. & Marshak, S. 1985. Disjunctive cleavage formed at shallow depths in sedimentary rocks. *J. Struct. Geol.* **7**, 327–343.

Funiciello, R., Parotto, M. & Praturlon, A. 1981. *Carta Tettonica d'Italia*. C.N.R., Roma.

Gamond, J. F. 1983. Displacement features associated with fault zones: a comparison between observed examples and experimental models. *J. Struct. Geol.* **5**, 33–45.

Gamond, J. F. & Giraud, A. 1982. Identification des zones de faille à l'aide des associations de fractures de second ordre. *Bull. Soc. géol. Fr.* **24**, 755–762.

Ghisetti, F. & Vezzani, L. 1986a. Assetto geometrico ed evoluzione strutturale della catena del Gran Sasso tra Vado di Siella e Vado di Corno. *Boll. Soc. geol. ital.* **105**, 131–171.

Ghisetti, F. & Vezzani, L. 1986b. *Carta Geologica del Gruppo M. Siella-M. Camicia-M. Prena-M . Brancastello (Gran Sasso d'Italia, Abruzzo)*. Scale 1:15.000. S.EL.CA., Firenze.

Koopman, A. 1983. Detachment tectonics in the central Apennines, Italy. *Geologica Ultraiect.* **30**, 1–155.

Lavecchia, G. 1985. Il sovrascorrimento dei Monti Sibillini: analisi cinematica e strutturale. *Boll. Soc. geol. ital.* **104**, 161–194.

Lister, G. S. & Williams, P. F. 1983. The partitioning of deformation in flowing rock masses. *Tectonophysics* **92**, 1–33.

Mandl, G., de Jong, L. N. & Maltha, A. 1977. Shear zones in granular material. An experimental study of their structures and mechanical genesis. *Rock Mech.* **9**, 95–144.

Marshak, S., Geiser, P. A., Alvarez, W. & Engelder, T. 1982. Mesoscopic fault array of the northern Umbrian Apennine fold belt, Italy: geometry of conjugate shear by pressure-solution slip. *Bull. geol. Soc. Am.* **93**, 1013–1022.

Morgenstern, N. R. & Tchalenko, J. S. 1967. Microscopic structures in kaolin subjected to direct shear. *Géotechnique* **17**, 309–328.

Parotto, M. & Praturlon, A. 1975. Geological summary of the Central Apennines. In: *Structural Model of Italy* (edited by Ogniben, L., Parotto, M. & Praturlon, A.). *C.N.R., Quaderni de la Ricerca Scientifica* **90**, 257–311.

Powell, C. McA. 1979. A morphological classification of rock cleavage. *Tectonophysics* **58**, 21–34.

Ramsay, J. G., Casey, M. & Kligfield, R. 1983. Role of shear in development of the Helvetic fold-thrust belt of Switzerland. *Geology* **11**, 439–442.